Supplementary file for

Ultrafast Magnetization Dynamics in FeCo Thin Films with Varied Stoichiometry

Tugce Bozdag[a,b], Bekir Asilcan Unlu[a, b], Metin Arslan[a], Eyup Kavak[a, b], Eyup Duman[a,c,1] , Halime Gul Yaglioglu[a,c,2]

[a]*Department of Engineering Physics, Ankara University, Degol Street, 06100 Besevler, Ankara (Turkiye)*

[b]*Graduate School of Natural and Applied Sciences, Ankara University, 06110 Dı¸skapı, Ankara, (Turkiye)*

[c]*Turkish Accelerator and Radiation Laboratory (TARLA), Bah¸celievler Mah. 306 sk. No: 11/N, 06830 Golbasi, Ankara (Turkiye)*

S1. Electron Microscopy Studies for deposited thin films

All thin films were deposited using 5-inch Fe and Co targets. The compositions of the deposited thin films were altered by changing the applied power to the Fe target. A series of thin film samples were deposited by adjusting the current to control the sputtering power. Figures S1–S3 show the BSE and SE images of the FeCo1, FeCo2 and FeCo3 thin films, respectively. The BSE images do not show any contrast, indicating that the chemical composition of the thin films are homogeneous.

For FeCo1 thin films: DC power for Fe: 40 W, DC power for Co target: 40 W

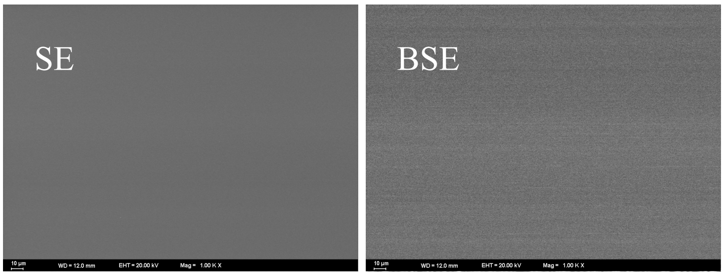

Figure S1. SE and BSE images of deposited so-called FeCo1 thin film.

For FeCo2 thin films: DC power for Fe: 60 W, DC power for Co target: 40 W

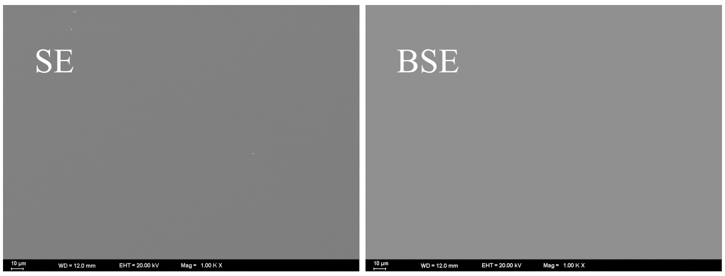

Figure S2. SE and BSE images of deposited so-called FeCo2 thin film.

For FeCo3 thin films: DC power for Fe: 70 W, DC power for Co target: 40 W

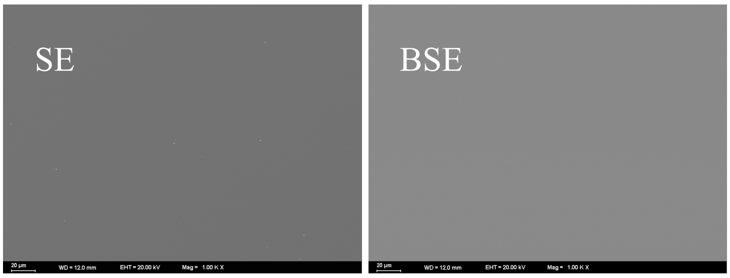

Figure S3. SE and BSE images of deposited so-called FeCo3 thin film.

The chemical composition of the deposited thin films was determined by using of an EDX detector. EDX spectra were collected from the marked region of the samples (purple rectangular in SE picture). The Figure S4, S5, S6 exhibit the EDX spectra of the FeCo1, FeCo2 and FeCo3 thin films, respectively. The obtained chemical compositions are writen in every EDX spectra. The elemental mapping of the region marked as purple rectangular are also given in the same figures. The elemental mapping of Fe and Co demonstrates that the chemical composition of the thin films are homogeneous across the entire surface of the film.

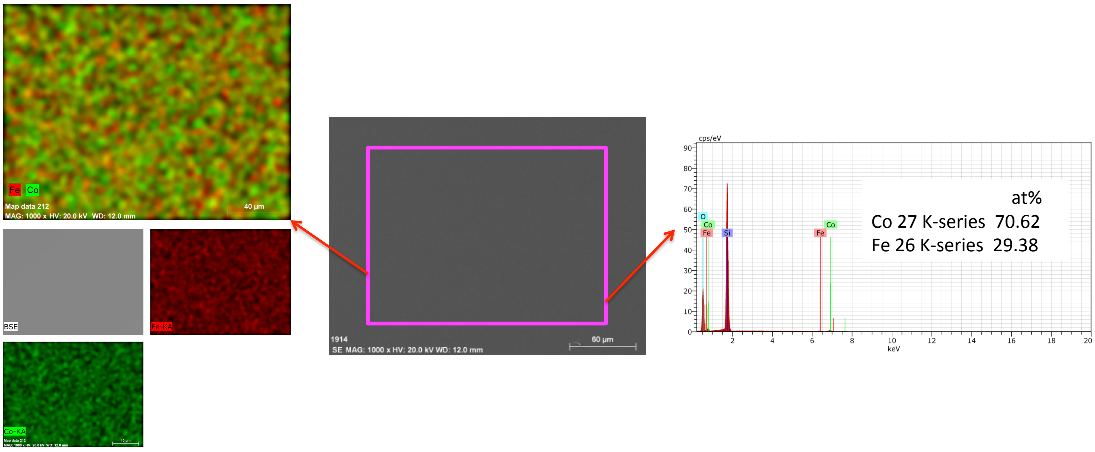

Figure S4 EDX spectrum and elemental mapping of deposited FeCo1 thin film. The obtained chemical composition is writen in EDX spectra.

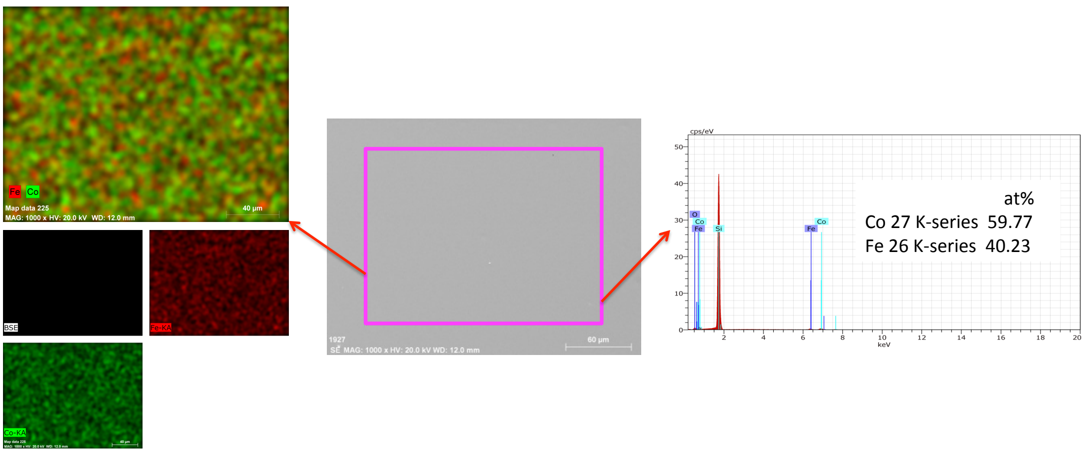

Figure S5. EDX spectrum and elemental mapping of deposited FeCo2 thin film. The obtained chemical composition is writen in EDX spectra.

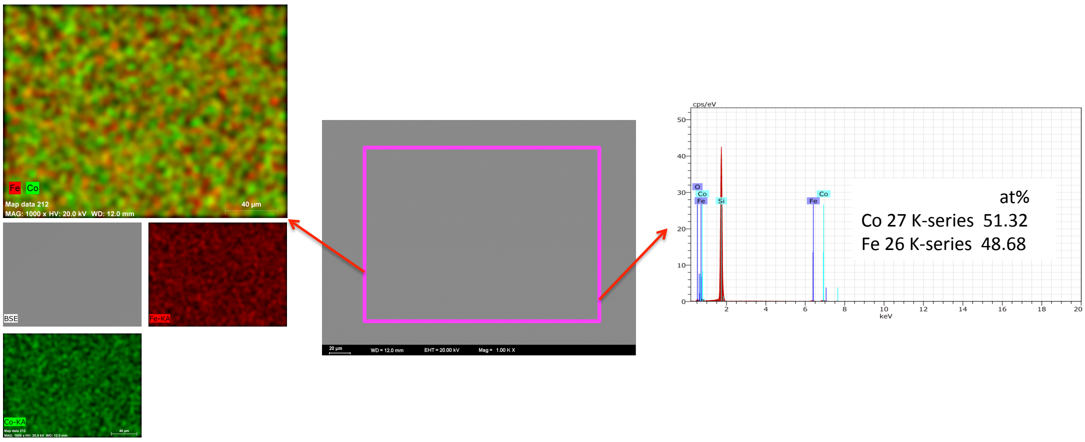

Figure S6. EDX spectrum and elemental mapping of deposited FeCo3 thin film. The obtained chemical composition is writen in EDX spectra.

S2. Fitting the experimental data to the analytical solution (AS) and 3TM Model to estimate of temperatures of three subsystems

The upper panels of Fig. S7,S8,S9 show how the temperature of the three subsystems change over time for specific laser fluences for all the studied samples. On the other hand, the lower panel of Fig.S7,S8,S9 show the fit results of the experimental TR-MOKE data for all the investigated samples, based on to Eq. 1 given in the main text.

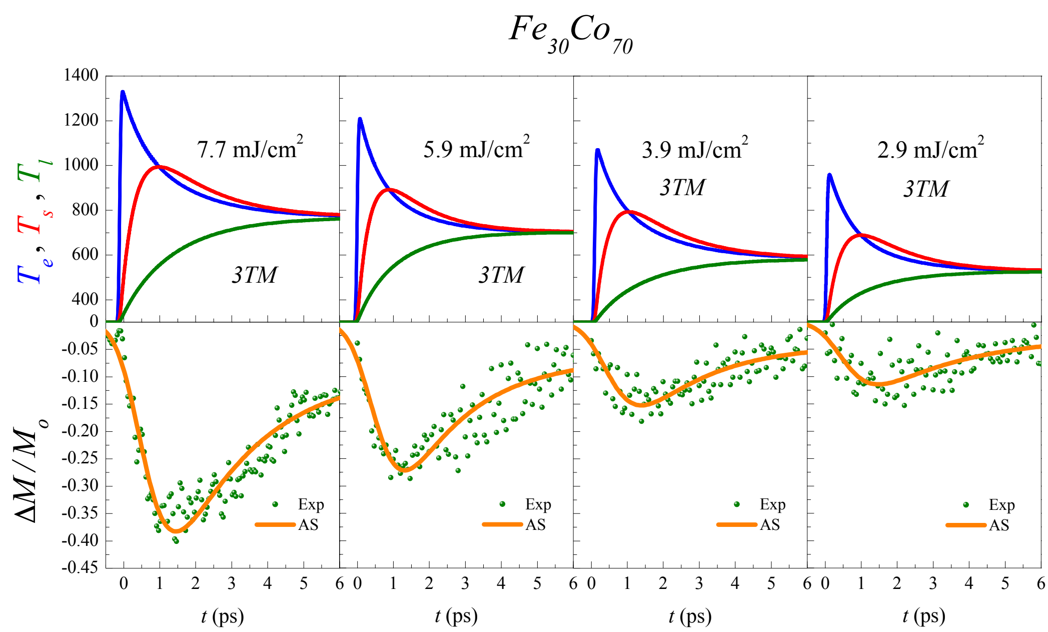

Figure S7 Upper panel: Temperol evolution of the temperature of electron, spin and lattice sub-systems for given fluence values in $Fe_{30}Co_{70}$ thin film. Lower panel: Fit results our TR-MOKE experimental data to a phenomenological equation, so called analytical solution (AS).

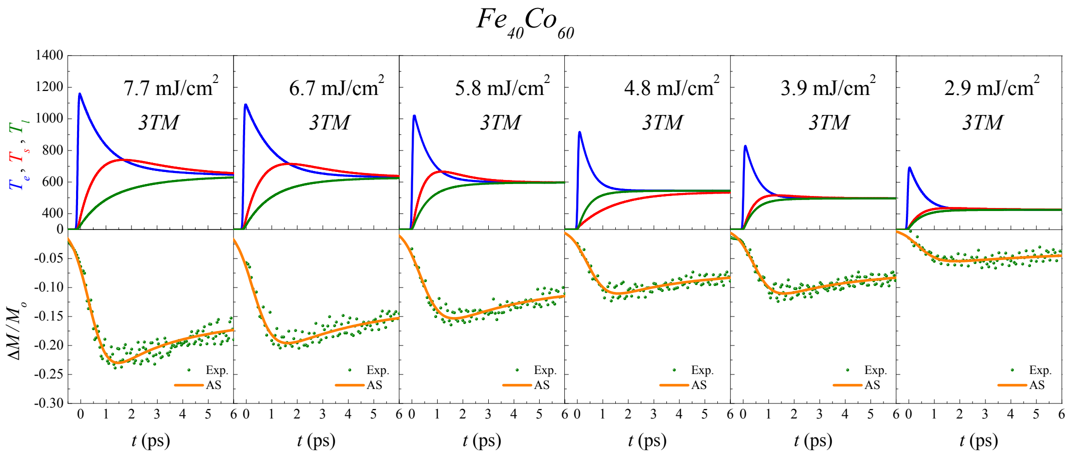

Figure S8 Upper panel: Temperol evolution of the temperature of electron, spin and lattice sub-systems for given fluence values in $Fe_{40}Co_{60}$ thin film. Lower panel: Fit results our TR-MOKE experimental data to a phenomenological equation, so called analytical solution (AS).

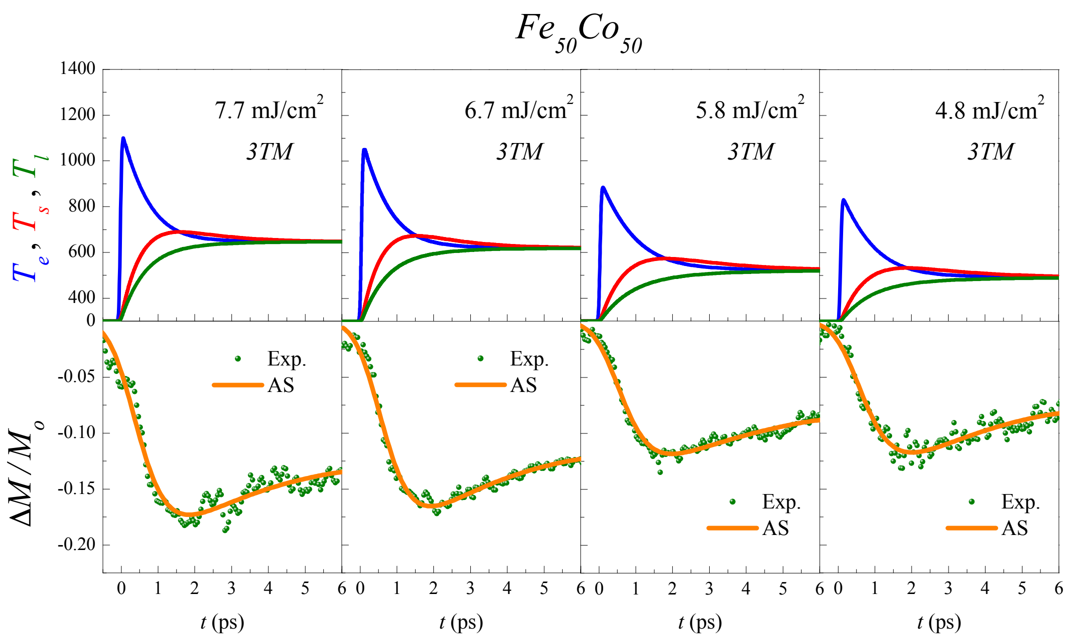

Figure S9 Upper panel: Temperol evolution of the temperature of electron, spin and lattice sub-systems for given fluence values in $Fe_{50}Co_{50}$ thin film. Lower panel: Fit results our TR-MOKE experimental data to a phenomenological equation, so called analytical solution (AS).

The parameters obtained by solving 3TM equations (given as Eq.2 in main text) are given in Table S1.

Thin films	f (mJ cm^{-2})	G_{es} (Js m^{-3}K^{-1})	G_{ep} (Js m^{-3}K^{-1})
$Fe_{30}Co_{70}$	2.9	2.11x10^{17}	2.10x10^{17}
	3.9	2.02x10^{17}	2.50x10^{17}
	5.8	2.21x10^{17}	2.70x10^{17}
	7.7	2.31x10^{17}	2.80x10^{17}
$Fe_{40}Co_{60}$	2.9	1.01x10^{17}	3.32x10^{17}
	3.9	1.32x10^{17}	3.28x10^{17}
	4.8	1.67x10^{17}	3.59x10^{17}
	5.8	1.69x10^{17}	3.79x10^{17}
	6.7	1.68x10^{17}	3.57x10^{17}
	7.7	1.59x10^{17}	3.66x10^{17}
$Fe_{50}Co_{50}$	4.8	1.04x10^{17}	2.24x10^{17}
	5.8	1.01x10^{17}	2.43x10^{17}
	6.7	1.32x10^{17}	3.31x10^{17}
	7.7	1.21x10^{17}	3.52x10^{17}

The G_{ep} and G_{es} values tends to increase with increasing fluence, which is another indication that underlying mechanism responsible for the ultrafast demagnetization in FeCo thin films is predominantly governed by the spin-flip process (S1).

References

S1. Suchetana Mukhopadhyay Sudip Majumder, Surya Narayan Panda and Anjan Barman, Investigation of ultrafast demagnetization and Gilbert damping and their correlation in different ferromagnetic thin films grown under identical conditions, Nanotechnology 34, 2023, 235702. doi: 10.1088/1361-6528/acc079